

Mechanism and Kinetics of Methylating C₆–C₁₂ Methylbenzenes with Methanol and Dimethyl Ether in H-MFI Zeolites

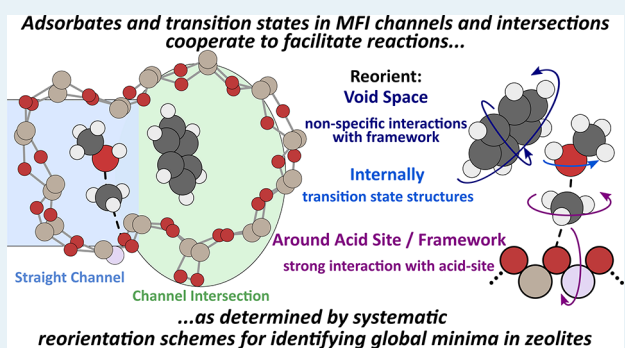
Mykela DeLuca, Pavlo Kravchenko, Alexander Hoffman,[✉] and David Hibbitts*[✉]

Department of Chemical Engineering, University of Florida, Gainesville, Florida 32611, United States

Supporting Information

ABSTRACT: This study uses periodic density functional theory (DFT) to determine the reaction mechanism and effects of reactant size for all 20 arene (C₆–C₁₂) methylation reactions using CH₃OH and CH₃OCH₃ as methylating agents in H-MFI zeolites. Reactant, product, and transition state structures were manually generated, optimized, and then systematically reoriented and reoptimized to sufficiently sample the potential energy surface and thus identify global minima and the most stable transition states which interconnect them. These systematic reorientations decreased energies by up to 45 kJ mol⁻¹, demonstrating their necessity when analyzing reaction pathways or adsorptive properties of zeolites. benzene–CH₃OCH₃ methylation occurs via sequential pathways, consistent with prior reports, but is limited by surface methylation which is stabilized by coadsorbed benzene via cooperativity between the channels and intersections within MFI. These coadsorbate-assisted surface methylations generally prevail over unassisted routes. Calculated free energy barriers and reaction energies suggest that both the sequential and concerted methylation mechanisms can occur, depending on the methylating agent and methylbenzene being reactant; no single mechanism prevails for these homologous reactions. Intrinsic methylation barriers for stepwise reactions of benzene to hexamethylbenzene remain between 75–137 kJ mol⁻¹ at conditions relevant to methanol-to-hydrocarbon (MTH) reactions where such arene species act as cocatalysts. Intrinsic methylation barriers are similar between CH₃OH and CH₃OCH₃, suggesting that both species are equally capable of interconverting methylbenzene species. Additionally, these methylation barriers do not systematically increase as the number of methyl-substituents on the arene increases and the formation of higher methylated arenes is thermodynamically favorable. These barriers are significantly lower than those associated with alkene formation during the aromatic cycle, suggesting that aromatic species formed during MTH reactions either egress from the catalyst—depending on that zeolite's pore structure—or become trapped as extensively substituted C₁₀–C₁₂ species, which can either isomerize to form olefins or ultimately create polyaromatic species that deactivate MTH catalysts.

KEYWORDS: surface methoxy (CH₃–Z), kinetics, zeolites, coadsorbate interactions, methanol-to-olefins, methylation



1. INTRODUCTION

Brønsted-acid-catalyzed alkylation reactions are ubiquitous, occurring during alcohol dehydration,^{1,2} alkene oligomerization,^{3,4} and methanol-to-hydrocarbon (MTH) reactions.^{5,6} Methanol does not directly couple to form C–C bonds during MTH reactions or does so at low rates.^{5,7–9} Instead, zeolite surfaces, alkenes, and arenes are methylated by a combination of methanol (CH₃OH) and dimethyl ether (CH₃OCH₃), both present at MTH conditions. Alkenes can grow through repeated methylation reactions (reacting with surface methoxy (CH₃–Z) species or directly with methylating agents such as CH₃OH and CH₃OCH₃). Larger C₆₊ alkenes can crack into C₂–C₄ alkenes which can desorb as products or realkylate in the alkene cycle, in which olefins are alkylated and crack to form other alkene species of varying lengths.^{10–15} For example, three CH₃OH molecules may sequentially methylate propene to form hexene which could crack into two propene molecules; as such, this olefin-forming process can be “auto-catalytic” as

alkenes are both cocatalysts and products of MTH. Alkenes may, instead of cracking, undergo hydride transfer reactions with other alkenes (to form alkanes and dienic compounds) or with methanol (to form alkanes, formaldehyde, and ultimately dienes) and then cyclize in mono- or bimolecular routes to ultimately form aromatic compounds (arenes).^{16,17} These arenes can be methylated during MTH to form one of 12 distinct C₇–C₁₂ methylbenzene species, shown in Figure 1. Many of these methylbenzene species can undergo isomerization and dealkylation reactions to produce light alkene products that can egress from the zeolite crystal or join the alkene cycle; thus, the alkene products from methylbenzenes may be incorporated into other aromatic compounds, again leading to autocatalytic behavior.^{18–21} Therefore, under-

Received: February 13, 2019

Revised: May 20, 2019

Published: May 23, 2019

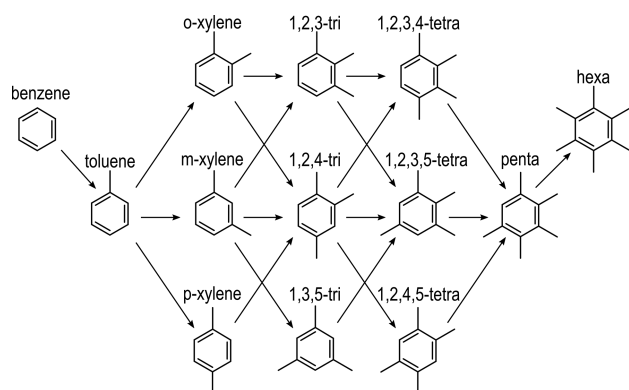
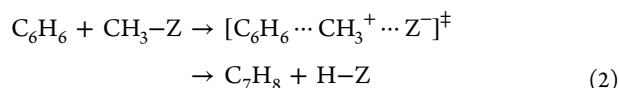
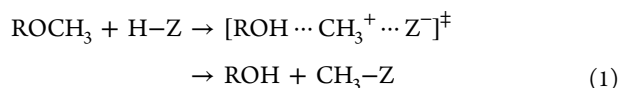


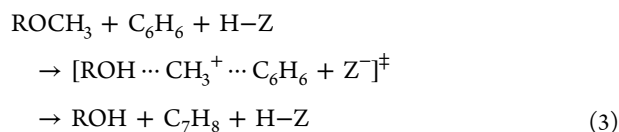
Figure 1. All possible methylation pathways of C_6 – C_{12} methylbenzene species.

standing how arene cocatalysts interconvert is key to understanding the larger MTH reaction network. Arene methylation, in addition to its role in MTH, is also important in the formation of toluene from benzene, toluene disproportionation to xylenes, and other transalkylation reactions.^{22–25} Despite the ubiquity of arene methylation reactions in industrial processes, there are few studies contrasting arene methylation mechanisms with CH_3OH and CH_3OCH_3 and fewer studies elucidating methylation mechanisms across a wide range of methylbenzene reagents.

Brønsted-acid-catalyzed alkylation reactions occur via one of two distinct mechanisms:^{6,26–31} a sequential mechanism (also known as the dissociative or indirect mechanism) or a concerted mechanism (also known as the associative or direct mechanism). In the sequential mechanism, the methylating agent first methylates the zeolite to form CH_3-Z preceding the methylation of an alcohol, alkene, or arene:



In the concerted mechanism, the methylating agent directly reacts with an alcohol, alkene, or arene:



Surface methoxy species are a reactive intermediate in the sequential pathway but not the concerted pathway, and their presence is commonly used to differentiate between these pathways. The purging of C_6H_6 – CH_3OCH_3 after reaction in a pillared MFI framework zeolite (H-SPP, 358 K) followed by a subsequent heat treatment (423 K) and titration with H_2O formed CH_3OH in a 1:1 ratio with Al, suggesting high surface methoxy coverages.²⁸ Benzene and toluene d_6 DME/DME switching experiments demonstrate a 1:2:1 ratio of d_6 : d_3 : d_6 indicating rapid C–O bond breaking and formation at reaction conditions,²⁸ consistent with alkene methylation studies.²⁹ However, CH_3-Z species were not identified by FT-IR during the coreaction of benzene and CH_3OH at 623 K at steady state—conditions that better represent those of MTH

processes²⁷—suggesting that the presence of an arene at reaction conditions may alter the amount of surface methoxy species formed. The absence, presence, or abundance of CH_3-Z , however, does not rule out either methylation mechanism. For instance, the absence or scarcity of CH_3-Z species can indicate that the concerted mechanism occurs (i.e., they are not formed) or that ring methylation consumes CH_3-Z too fast for them to accumulate to detectable levels. Similarly, high coverages of CH_3-Z species do not preclude the concerted mechanism from occurring, as CH_3-Z species may be unreactive spectators in arene methylation or react predominantly with oxygenates.

The sequential and concerted mechanisms may also differ by the kinetic dependencies of the methylating agent (CH_3OR), the leaving group (ROH), and the species being methylated (alcohol, alkene, or arene). Kinetic studies (0.002–0.05 bar aromatic, 0.29–0.68 bar CH_3OCH_3 , 0.1% conversion) of benzene (373 K), toluene (403 K), and xylene (473 K) methylation with CH_3OCH_3 have shown rates independent of CH_3OCH_3 pressure and linearly dependent on arene pressure.²⁸ Coupled zero-order effects of CH_3OCH_3 and first-order effects of arene reagents suggest that sequential methylation pathways prevail and are limited by arene methylation steps on surfaces covered by CH_3-Z species; however, coadsorbate-assisted surface methylation reactions have not been considered.²⁸ Density functional theory (DFT) calculations on a cluster of four tetrahedral sites (T-sites) and ab initio molecular dynamic studies indicate concerted methylation barriers are >30 kJ mol^{−1} lower than those of sequential methylation with CH_3OCH_3 .^{32,33} These theoretical data suggest that benzene methylation proceeds via concerted methylation;^{28,29} however, small cluster models fail to adequately model periodic zeolite catalysts and do not capture the critical dispersive interactions in zeolite pores that stabilize guest species.³⁴ There is an apparent disparity between computational studies and experimental studies regarding the coverage and role of CH_3-Z species and the route by which arenes are methylated.

Theoretical and experimental work has demonstrated that CH_3OCH_3 methylates alkenes and arenes at a faster rate than CH_3OH . CH_3OCH_3 methylates propene at a rate 2.5 times faster than CH_3OH in H-ZSM-5 (523 K, 0.02 bar propene, 0.025–0.075 bar CH_3OH or CH_3OCH_3).¹¹ DFT calculations on cluster models with four T-sites similarly predict that concerted methylation of both propene and toluene occur with lower barriers from CH_3OCH_3 than with CH_3OH .¹¹ Computational and experimental studies generally agree that CH_3OCH_3 is the dominant methylation agent at typical arene methylation conditions (low conversions, 400–600 K).^{35–37} These comparisons between CH_3OH and CH_3OCH_3 are limited to methylations of C_6 – C_8 arenes; larger, extensively substituted methylbenzene species, however, may crowd out CH_3OCH_3 molecules in favor of smaller CH_3OH , thereby limiting the effectiveness of CH_3OCH_3 during methylation.

Few studies investigate the effects of arene substitution on methylation barriers and preferred methylation mechanisms. DFT calculations of *p*-xylene, 1,2,4-trimethylbenzene, and 1,2,3,5-tetramethylbenzene on larger 66 T-sites of H-ZSM-12 and H-ZSM-22 suggest that barriers of concerted methylation by CH_3OH remain relatively constant for C_8 and C_9 species but increase for C_{10} species—suggesting that strong repulsive interactions limit methylation in these zeolites.³⁸ Additionally, this work demonstrated that in H-ZSM-22 geminal methyl-

ation of the C₁₀ species was more favorable than C–H methylation, suggesting that dimethylated C₁₁ species will participate in the aromatic cycle in H-ZSM-22. DFT calculations on a four T-site cluster model predicted that concerted CH₃OH-arene methylation barriers were 191 kJ mol⁻¹, 174 kJ mol⁻¹, and 171 kJ mol⁻¹ for toluene, 1,2,4,5-tetramethylbenzene, and hexamethylbenzene, leading to the conclusion that methylation barriers decrease as the number of methyl substituents increases.³⁹ Conversely, the rates of *o*- and *p*-xylene methylation (473 K, 0.05 bar xylene, 0.1% conversion, 0.68 bar CH₃OCH₃) in H-ZSM-5 were lower than those for benzene (373 K, 0.02 bar benzene, 0.1% conversion, 0.68 bar CH₃OCH₃); however, differences in temperature and the mass transport properties of these reactants make direct comparisons more difficult.²⁸ A possible cause for the discrepancy between theoretical and experimental results regarding the effects of methyl-substitution on arene methylation could be the lack of confinement effects—responsible for lowering the methylation barriers of smaller arenes through non-covalent stabilization and raising the methylation barriers of larger arenes through repulsive interactions—in cluster calculations. Zeolite models with fully periodic boundary conditions can overcome the limitations of cluster calculations, but to our knowledge, arene methylation has not been rigorously investigated using fully periodic models.

Here, we use fully periodic density functional theory (DFT) calculations to investigate the methylation of all possible methylbenzene cocatalysts via the concerted and sequential mechanisms with methylating agents CH₃OH and CH₃OCH₃ in H-MFI. Systematic reorientations were performed on all states to sample the potential energy surface in an attempt to identify the global minimum for each state, rather than local minima obtained from single optimizations. Sampling the potential energy surface using this method is crucial to obtain reliable results in ground-state theoretical zeolite studies, as energies decreased by up to 45 kJ mol⁻¹ after systematically reorienting species. We also show that benzene methylation occurs via the sequential mechanism, consistent with experimental results, and that the rate is limited by the formation of CH₃-Z, which occurs in the presence of adsorbed benzene. Co-localized arene species stabilize surface methylation transition states through additional dispersive interactions, cooperating with the surrounding zeolite framework to stabilize these structures. These results provide insight into the unique reactivity of MFI as enabled by the joining of diverse channel and intersection environments. Stepwise methylation barriers of benzene to hexamethylbenzene, relevant to MTH reactions, indicate that these reactions are relatively facile and the formation of higher methylated species is thermodynamically favorable, suggesting that aromatic species formed during MTH reactions either escape zeolite domains or become trapped as C₁₀–C₁₂ methylbenzene species which can cocatalyze olefin formation or lead to catalyst deactivation.

2. METHODS

2.1. Computational Methods. DFT calculations were carried out using the Vienna ab initio simulation package (VASP)^{40–43} in a fully periodic MFI unit cell. Planewaves were constructed using projector augmented-wave (PAW)^{44,45} potentials with an energy cutoff of 400 eV. The Perdew–Burke–Ernzerhof (PBE) form of the generalized gradient approximation (GGA) was used to determine exchange and

correlation energies.^{46–48} The DFT-D3 method with Becke and Johnson damping accounted for dispersive interactions.^{49–51} The Brillouin zone was sampled at the Γ -point for all calculations.⁵²

The MFI structure was obtained from the IZA database⁵³ and annealed using ab initio molecular dynamics (AIMD) to generate a low-energy state for these DFT settings. The structure was heated from 200 to 800 K over 3000 fs, held at 800 K for 3000 fs, and then cooled over 15000 fs. During these AIMD studies, the wave function for each step was converged to within 10⁻⁴ eV and one atom was fixed to prevent bulk translation. The final structure obtained after annealing and optimizing is 23 kJ mol⁻¹ more stable than the directly optimized IZA structure (Figure S1, in the [Supporting Information](#), SI). These calculations were done to ensure stability within the baseline framework and to prevent framework restructuring from altering calculated activation and reaction energies, as described in detail elsewhere.⁵⁴ Previous work investigating methanol dehydration on sites T3, T10, T11, and T12 in MFI suggests that surface methylation occurs with the lowest barriers at T11;² therefore, all calculations were performed at the T11 T-site in MFI, which gives access to both the straight channel and the channel intersection where arenes prefer to adsorb.

All reactant, product, and transition states were optimized with static DFT calculations until the maximum force on any atom was <0.05 eV Å⁻¹. Wave functions were converged to within 10⁻⁶ eV, and all forces were computed using a fast Fourier transform (FFT) grid with a cutoff twice the planewave cutoff. No atoms were constrained in any DFT optimization, pathway, or transition state calculations while the lattice parameters (*a* = 20.090 Å, *b* = 19.738 Å, *c* = 13.142 Å) and orthorhombic shape were fixed.

Minimum energy pathways were estimated using the nudged elastic band (NEB)^{55,56} method. NEB calculations used 16 images, and wave functions converged to 10⁻⁴ eV with an FFT grid 1.5 times the size of the plane-wave cutoff. The maximum force on each atom in all images was converged to <0.5 eV Å⁻¹. This estimate of the minimum energy pathway was used to generate initial transition state structures and reaction modes for the Dimer method,⁵⁷ which optimizes a pair of structures to determine the local curvature of the potential energy surface until ultimately converging on a saddle point. The same convergence criteria were used for optimization and dimer calculations (e.g., maximum forces on any atom <0.05 eV Å⁻¹).

Frequencies were calculated for all reactant, product, and transition states using a fixed displacement method where the adsorbates (e.g., CH₃OH and benzene) and AlO₄H of the acid site are displaced while all other framework atoms are fixed. Low-frequency modes (<60 cm⁻¹) were replaced with 60 cm⁻¹, similar to previous work,^{58,59} because low frequencies are inaccurate and contribute significantly to vibrational entropy terms. These frequency calculations are used to determine temperature-corrected (373–673 K) enthalpies and free energies according to harmonic oscillator approximations for vibrational partition functions and ideal gas treatments of rotational and translational partition functions for bulk gas species.

2.2. Reorientations of Reactant, Product, and Transition States. All DFT-optimized reactant, product, and transition states were systematically reoriented and reoptimized to increase the likelihood that optimum transition

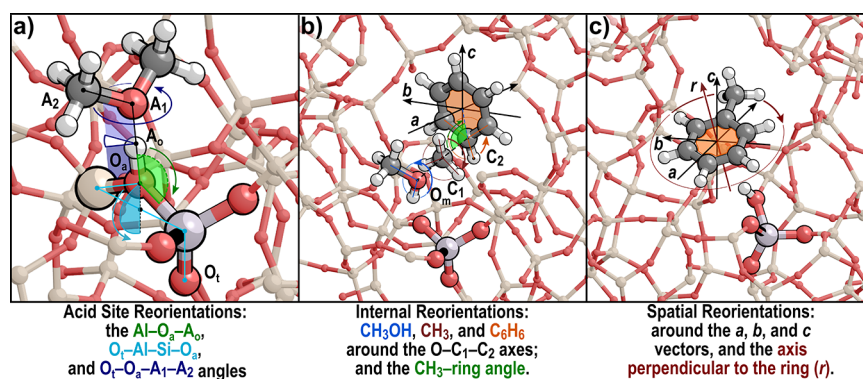


Figure 2. (a) Three different acid site reorientations about the $\text{Al}-\text{O}_a-\text{A}_1$ angle (green), $\text{O}_t-\text{Al}-\text{Si}-\text{O}_a$ angle (cyan), and $\text{O}_t-\text{O}_a-\text{A}_1-\text{A}_2$ angle (blue). (b) Internal reorientations of the concerted transition state where CH_3OH (blue), CH_3 (brown), and C_6H_6 can be rotated about the $\text{O}_m-\text{C}_1-\text{C}_2$ angle formed between the leaving group, the adding CH_3 , and the ring (orange). The angle of the ring can be altered relative to the adding CH_3 group by altering the CH_3 -ring angle (green). (c) Spatial reorientations of methylbenzene about the a-, b-, and c-axes of the unit cell and the axis perpendicular to the center of the ring (red). Larger versions of each image are available, for clarity, in the [Supporting Information](#) (Figures S2–S4).

state structures were obtained via static (nondynamic) DFT calculations. Species were first optimized from manually generated structures and then reoriented based on the nature of the interaction between the adsorbate and the zeolite; all reoriented structures are subsequently reoptimized to identify minimum energy states. Adsorbed species and transition states can interact with the zeolite in several ways: forming covalent bonds (e.g., CH_3-Z), forming H-bonds with Brønsted acid sites (e.g., CH_3OH^*), or purely through nonspecific dispersive and electrostatic interactions (e.g., C_6H_6^* , $\text{C}_7\text{H}_9^{+*}$). Three reorientation schemes are used here: acid site reorientations, internal reorientations, and spatial reorientations (Figure 2 gives examples of all three).

Adsorbates that covalently bind to the framework or form H-bonds with protonated Brønsted acid sites, such as adsorbed oxygenates and alkoxides, underwent acid site reorientations (e.g., $\text{CH}_3\text{OCH}_3^*$ in Figure 2a). Structures and acid sites are rotated by altering the dihedral angle formed between an O atom of the acid site (O_t), the Al atom, the Si atom closest to the acid site, and the O to which the proton or alkoxide is bound (O_a) in $\text{O}_t-\text{Al}-\text{Si}-\text{O}_a$ rotations. This motion effectively sweeps the adsorbed species around the acid site (Figure 2a), as done previously for Brønsted acid site calculations.⁶⁰ The $\text{O}_t-\text{Al}-\text{Si}-\text{O}_a$ angles were varied by 30° increments from 30° – 330° , and each 30° increment was optimized using the parameters discussed in Section 2.1. The angle between the Al atom, the O_a atom, and the adsorbate itself (A_1) can also be varied (Figure 2a) to move the adsorbate above the acid site parallel to the $\text{Si}-\text{O}_a-\text{Al}$ bridge, and this $\text{Al}-\text{O}_a-\text{A}_1$ angle was varied by -30° , -15° , 15° , and 30° from the initial optimized position and optimized at all of these increments. Finally, the dihedral angle between a T-site, the O_a atom, and two adsorbate atoms (A_1 and A_2) can be altered to spin the adsorbate around the O_a atom, as shown in Figure 2a, the dihedral angles were varied by 30° increments from 30° to 330° , and each 30° increment was optimized using the parameters discussed in Section 2.1.

Large transition state complexes associated with surface methylation, sequential methylation of the arene ring, or concerted methylation of the arene ring have multiple fragments that can rotate about breaking or nascent bonds. Concerted benzene methylation by CH_3OCH_3 , for example, involves CH_3OH , methyl, and arene fragments (Figure 2b),

and these species can be reoriented relative to one another to isolate more stable transition state structures. The orientation of the ring relative to the attacking methyl group (ring- CH_3 angle) was altered so that the two species were coplanar. Furthermore, the ring was rotated about the axis of the oxygen of the CH_3OH group (O_m), the carbon of the attacking methyl species (C_1), and the carbon on the ring being attacked (C_2) so that the orientation of the ring changes without affecting the incipient bond of the transition state. Rotations about the $\text{O}_m-\text{C}_1-\text{C}_2$ axis were performed from 30° to 330° in 30° increments, and each 30° increment was optimized using the parameters discussed in Section 2.1. This transition state complex, furthermore, can be rotated spatially as it interacts nonspecifically with the zeolite framework and the deprotonated Brønsted acid site. Each transition state reorientation is reoptimized using the Dimer method. The mode and internal geometry of the initial structure is preserved during reoptimization (Figure S5), and all reoriented structures demonstrate a single strongly negative frequency associated with the expected bond-breaking or forming events.

Adsorbate species that interact nonspecifically through a combination of dispersive and electrostatic interactions and without H-bonds to a protonated acid site were rotated in spatial reorientations (e.g., methylbenzene in Figure 2c). Arenes were also rotated around the axis perpendicular to the ring (Figure 2c). Species were rotated and then optimized in 30° increments from 30° to 330° during these spatial reorientations; rotations resulting in collisions with the zeolite framework were discarded.

All reorientations described above are used as initial structures—they are not intended to determine torsional barriers or generate intramolecular potential energy surfaces; they are instead fully optimized in unconstrained calculations. As such, these reorientations serve to extensively seed a potential energy surface with multiple initial structures—each optimized—to potentially many local minima. These local minima are compared, and the minimum potential energy structures are used in further analysis. The relationship between the potential energy and free energy was tested for two states (C_6H_6^* and surface methylation near 1,2,4-trimethylbenzene transition state) by running frequency calculations for all reoriented structures. The results suggest that there is generally a strong correlation between potential

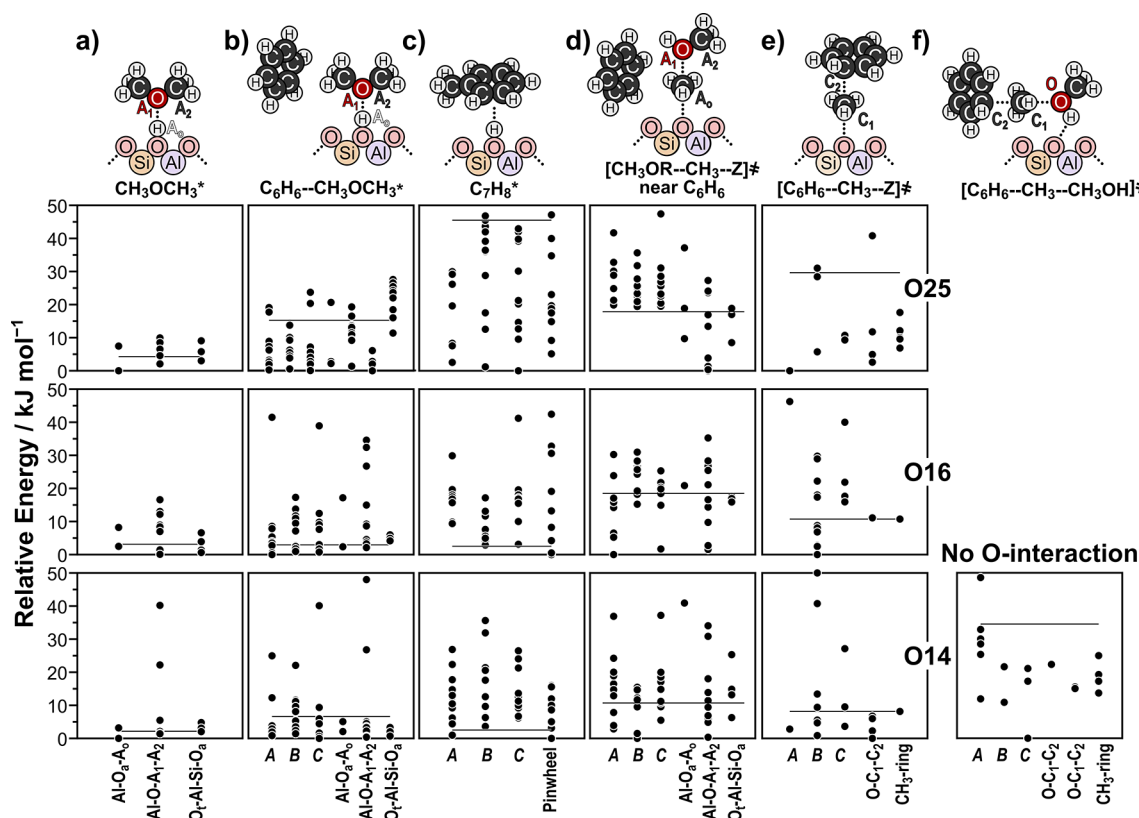


Figure 3. Dots represent the energies obtained from optimizing spatial reorientations (*a*-, *b*-, and *c*-axes), acid site reorientations ($\text{Al}-\text{O}_a-\text{A}_i$, $\text{Al}-\text{O}-\text{A}_1-\text{A}_2$, and $\text{O}_t-\text{Al}-\text{Si}-\text{O}_a$), and internal reorientations ($\text{O}-\text{C}_1-\text{C}_2$ and CH_3 -ring) performed on (a) $\text{CH}_3\text{OCH}_3^*$; (b) $\text{C}_6\text{H}_6\text{-CH}_3\text{OCH}_3^*$; (c) C_7H_8^* ; (d) the surface methylation transition state with CH_3OCH_3 ; (e) the ring methylation transition state at O14, O16, and O25; and (f) the concerted transition state, which does not covalently interact with an O-site, so reorientations are not O-dependent. All energies are relative to the most stable state at each respective O-site and reported in kJ mol^{-1} . The solid line represents the energy of the initial structure prior to reorientation.

energy and free energy (Figure S6 and S7). These reorientation techniques result in energies more accurate than those obtained from a single or small ensemble of DFT optimizations; however, they are not guaranteed to isolate global minima.

3. RESULTS AND DISCUSSION

3.1. Identifying the Most Stable Orientations and Locations of Arene Methylation Species. The T11 T-site is used for all reactions in this study and is connected to four unique O-sites: O14 (straight channel), O16 (intersection), O24 (beneath intersection), and O25 (intersection) (see Figure S8 in the Supporting Information). The O24 site is inaccessible for species larger than $-\text{CH}_3$, and therefore, all other reactions were studied only at O14, O16, and O25, except for surface methylation, which was modeled at all sites.

Systematic reorientations can find structures drastically lower in energy than initial optimizations (Figure 3). Three types of systematic reorientations were performed on guest species using static DFT calculations as appropriate: acid site, spatial, and internal reorientations. Each type of reorientation produced structures that were more stable than their manually generated counterparts. Figure 3 shows a subset of the results of the reorientations performed for $\text{CH}_3\text{OCH}_3^*$, $\text{C}_6\text{H}_6\text{-CH}_3\text{OCH}_3^*$, C_7H_8^* , the transition state for surface methylation in the presence of benzene, the transition state for benzene methylation from a surface methoxy, and concerted benzene methylation on each accessible O-site on T11.

Acid site reorientations were performed on adsorbates that covalently bind to the framework and those that form H-bonds to surface protons (e.g., $\text{CH}_3\text{OCH}_3^*$) as described in Section 2.2. Structures were reoriented by altering the $\text{O}_t-\text{Al}-\text{Si}-\text{O}_a$, $\text{Al}-\text{O}_a-\text{A}_1$, and $\text{O}_t-\text{O}_a-\text{A}_1-\text{A}_2$ angles (Figure 2a). These reorientations resulted in average energy decreases of 6.5 kJ mol^{-1} , 6.1 kJ mol^{-1} , and 11.3 kJ mol^{-1} compared to manually generated optimized structures for species relevant to benzene methylation. Figure 3a shows reorientations of $\text{CH}_3\text{OCH}_3^*$ about O14, O16, and O25 resulting in energy decreases of $\sim 6 \text{ kJ mol}^{-1}$ at each acid site.

Spatial reorientations were performed on species that do not strongly interact with the Brønsted acid site (e.g., toluene). The subset of structures relevant to benzene methylation were rotated about the *a*-, *b*-, and *c*-axes of the unit cell resulting in an average decrease in energy of 8.5 , 7.2 , and 8.4 kJ mol^{-1} , respectively. Species with one or more methyl-substituents on the benzene ring (toluene to hexamethylbenzene) were also rotated about the axis perpendicular to the center of the ring resulting in $< 5 \text{ kJ mol}^{-1}$ energy decreases for C_7H_8^* at O14 and O16 but a $\sim 45 \text{ kJ mol}^{-1}$ decrease at O25 (Figure 3c).

States with coadsorbed species, such as $\text{C}_6\text{H}_6\text{-CH}_3\text{OCH}_3^*$ (Figure 3b), may contain both acid-site interacting fragments ($\text{CH}_3\text{OCH}_3^*$) and noninteracting fragments (C_6H_6). These two fragments were rotated independently of each other. Benzene was rotated with spatial reorientations (e.g., Figure 2c), and CH_3OCH_3 was rotated with acid site reorientations (e.g., Figure 2a). The reorientation that located the minimum

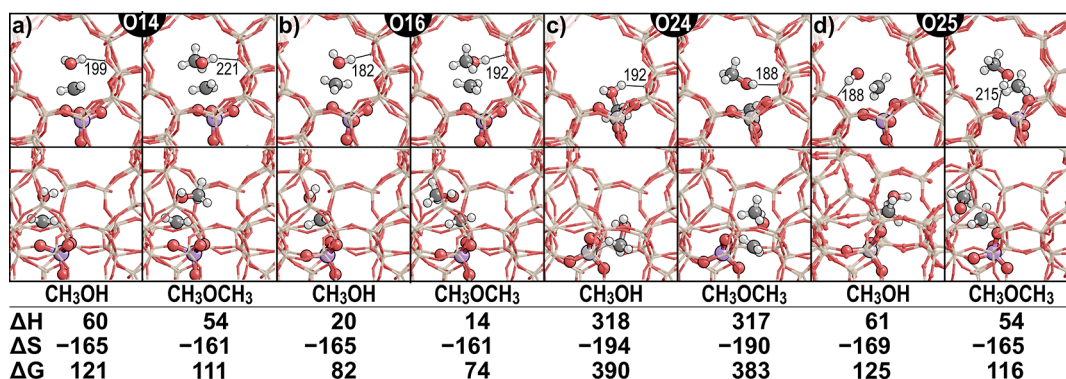


Figure 5. Lowest energy orientation of the surface methylation transition state at (a) O14, (b) O16, (c) O24, and (d) O25 looking down the straight (top) and sinusoidal (bottom) channels for CH₃OH and CH₃OCH₃. Enthalpy (kJ mol⁻¹), entropy (J mol⁻¹ K⁻¹), and free energy (kJ mol⁻¹) values are reported at 373 K and relative to a protonated zeolite and stoichiometric amounts of gas-phase CH₃OH or CH₃OCH₃ molecules, as appropriate. Relevant H-bond lengths are reported in pm. Additional viewing angles for the methylation of O24 are provided in Figure S11 in the Supporting Information.

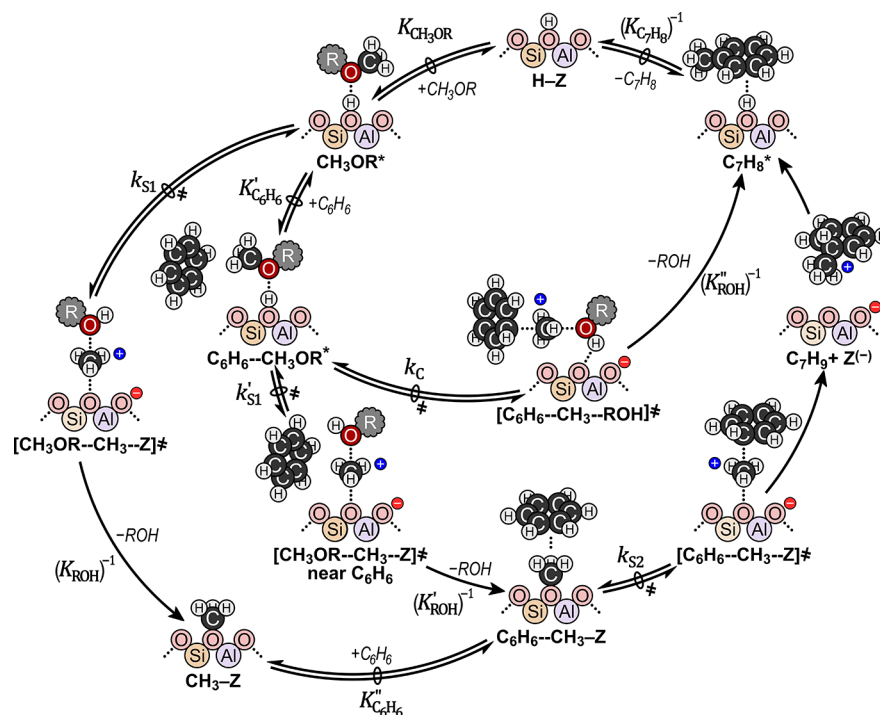


Figure 6. Scheme of benzene methylation pathways showing surface methylation with no spectating species, surface methylation with spectating benzene, concerted methylation, and deprotonation (left to right). Associated rate constants (K and k values) are shown adjacent to each arrow and are used in eq 4.

compared to determine the preferred mechanism. Maximum rate analyses can be used to compare reactions that occur in parallel, for example surface methylation in an empty pore versus surface methylation with a spectating arene, by identifying the mechanism with the highest maximum rate which is most likely to form the product. Alternatively, the maximum rate of reactions that occur in series—for example surface methylation followed by ring methylation of the sequential mechanism—is determined by identifying the step with the lowest maximum rate which limits the rate of that pathway. Maximum rate analysis also allows for comparison of DFT-derived rates and experimentally measured rates. We compare our predictions (Figure 7) to measurements obtained from kinetic studies of benzene methylation by CH₃OCH₃

(373 K, 0.02 bar aromatic, 0.68 bar CH₃OCH₃, 0.1% aromatic conversion).²⁸

Surface methoxy formation, the first step of the sequential mechanism, was investigated in an empty zeolite and with a spectating benzene ring with CH₃OH and CH₃OCH₃ at all four O-sites surrounding T11. Site O16, which is located in the channel intersection, has the lowest surface methoxy formation barrier with CH₃OH and CH₃OCH₃ (Section 3.1). At 353–463 K, surface methylation with spectating benzene occurs with a higher maximum rate than surface methylation in an empty pore by CH₃OH and CH₃OCH₃, demonstrating that benzene enthalpically stabilizes the surface methylation transition states (Figure 7b). The rate increase with a spectating benzene is accompanied by concomitant decreases in the intrinsic free energy barriers at these temperatures:

O-site to form $\text{CH}_3\text{-Z}$ species. Systematic reorientations suggest that the lowest barrier transition state occurs when the benzene ring is oriented so that it is coplanar with the attacking methyl group (Figure 8e). The transition state for arene methylation via $\text{CH}_3\text{-Z}$ is the same for CH_3OH and CH_3OCH_3 methylating agents; however, different ROH leaving groups for the two methylating agents yield different maximum rates. Differences in the formation and desorption energies of these ROH species—resulting from entropic contributions of the leaving group upon desorption—cause the maximum rate of arene methylation to be higher than that of surface methylation at temperatures >353 K (temperatures relevant to arene methylation and MTH). This indicates that the rate of sequential methylation is limited by $\text{CH}_3\text{-Z}$ formation and that the maximum rate of the consumption of $\text{CH}_3\text{-Z}$ is rapid relative to their formation at 0.1% conversion.

The pressure of the ROH leaving group, and thus the conversion, can alter the rate-determining step of the sequential mechanism. Arene methylation reactions are typically run at low arene conversions (0.1% here), and thus the pressure of ROH leaving group (0.00002 bar) is very low relative to the pressure of CH_3OR (0.68 bar). Rates of surface methylation are not dictated by ROH pressures at negligible conversions, where equilibrium effects need not be considered. Rates of arene methylation via $\text{CH}_3\text{-Z}$, however, are inhibited by ROH pressures and thus dependent on conversion, X

$$r = k_{S2}K_{\text{CH}_3\text{OR}}K'_{\text{SI}}K'_{\text{C}_6\text{H}_6}P_{\text{C}_6\text{H}_6,0} \frac{(1-X) \left(\frac{P_{\text{C}_6\text{H}_6,0}}{P_{\text{CH}_3\text{OR},0}} - X \right)}{X} \quad (4)$$

Increasing the conversion from 0.1% to 0.2% would cause a $\sim 2\times$ decrease in the rate of ring methylation via the sequential mechanism whereas the same conversion increase would negligibly impact rates if the concerted mechanism or surface methylation were the rate-determining steps (rate constants for eq 4 are defined in Figure 6 and derived in Section S2). As the pressure of the ROH group increases with increasing conversion, the formation and subsequent desorption of the ROH leaving group results in an inhibition of the benzene methylation through the action of Le Chatelier's principle. The rate of surface methoxy formation will approach equilibrium, thus limiting consumption of surface methoxy species by benzene and decreasing the rate of arene methylation (Figure 9, gray). This kinetic behavior is also observed, for example, in the hydrogenolysis of alkanes on metal surfaces, in which $\text{H}_2(\text{g})$ is formed in quasi-equilibrated dehydrogenation steps prior to the rate-determining C–C bond activation.^{61–63} At benzene conversions above $\sim 20\%$ for CH_3OH and CH_3OCH_3 , the rate of $\text{CH}_3\text{-Z}$ consumption by benzene becomes limited to the extent that benzene methylation becomes rate determining in the sequential pathway (Figure 9). At very high benzene conversions ($>75\%$) for CH_3OCH_3 , the concerted pathway occurs with nearly identical rates to the sequential pathway. These strong effects of ROH pressure at low conversion are only observed if sequential arene methylation is the rate-determining step (i.e., the rate is dependent on the pressure of ROH), lending importance to those experimental studies for this and similar methylation reactions (e.g., alcohol dehydration).¹ This inhibition via Le Chatelier's principle, unlike site-blocking inhibition, is observable across all pressure ranges of the ROH leaving group,

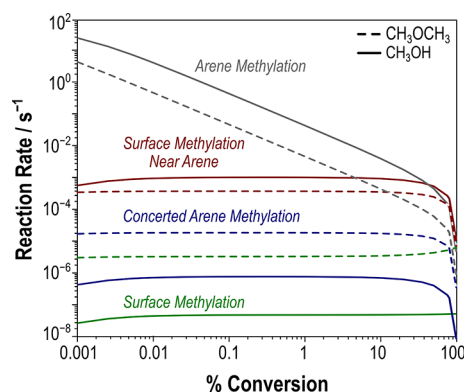


Figure 9. Rate of arene methylation (gray), surface methylation near arene (red), concerted methylation (blue), and surface methylation in an empty pore (green) with CH_3OH (solid lines) and CH_3OCH_3 (dashed lines) from 0.1–100% CH_3OR conversion at 0.68 bar CH_3OR , 0.02 bar C_6H_6 , 373 K.

indicating that it can be observed or ruled out by simple space velocity experiments, rarely published but often performed.

Concerted methylation and surface methylation with spectating benzene demonstrate the same pressure dependencies in the rate equation (eqs S7 and S19), rendering kinetic experiments incapable of differentiating the two mechanisms, thus motivating this DFT study. The most favorable orientation of the concerted methylation transition state involves a hydrogen bond between deprotonated O16 and the leaving group species (H_2O or CH_3OH , Figure 8f,g). Concerted methylation of benzene by CH_3OCH_3 (122 kJ mol^{-1}) is slightly more favorable than methylation by CH_3OH (129 kJ mol^{-1}); however, these values fall within the uncertainty of DFT, indicating that the relative rates of methylation by these two species should be nearly proportional to their pressure ratios. Free energy barriers of concerted methylation can be directly compared to those of the rate-determining surface methylation step as the two reactions demonstrate the same pressure dependencies. Barriers of concerted methylation are 20 kJ mol^{-1} higher for CH_3OH and 30 kJ mol^{-1} higher for CH_3OCH_3 than the barriers of surface methylation (Figure 7a), indicating that sequential methylation is the preferred mechanism at benzene methylation conditions. However, at conversions above 75% for CH_3OCH_3 the maximum rate of the sequential mechanism (determined by the maximum rate of arene methylation, Figure 9) is limited and the concerted mechanism becomes preferred as arene methylation rates from $\text{CH}_3\text{-Z}$ decrease.

Only direct proton donation from C_7H_5^+ to the zeolite surface was modeled to approximate ring deprotonation barriers. In a real system, CH_3OH and H_2O can act as proton shuttles and facilitate proton transfer to the zeolite surface and the barriers in the presence of these species could be lower. The rate of deprotonation, however, is significantly higher than the rate of other possible rate-determining steps for benzene methylation (Figure S12). Deprotonation benefits from relatively low barriers (Figure 7) coupled with entropic contributions of oxygenate desorption. As such, it does not limit methylation rates and will not be discussed in the remainder of this work because of its kinetic irrelevance.

Most abundant surface intermediates (MASI) were calculated using a Langmuir adsorption model, using DFT-obtained adsorption energies to identify abundant surface

intermediates. Possible MASI are limited to CH_3OR^* , C_6H_6^* , $\text{CH}_3\text{-Z}$, $\text{C}_6\text{H}_6\text{-CH}_3\text{OR}^*$, and $\text{C}_6\text{H}_6\text{-CH}_3\text{-Z}$ in this analysis. CH_3OH^* is the predominant MASI from 353–473 K when CH_3OH serves as the methylation agent. At temperatures above 473 K, the MASI becomes $\text{CH}_3\text{-Z}$, suggesting that surface methylation occurs in an empty pore at these temperatures, likely because adsorption of C_6H_6 is limited as the temperature increases (Figure S13). When CH_3OCH_3 serves as the methylation agent, $\text{C}_6\text{H}_6\text{-CH}_3\text{OCH}_3$ is the MASI between 353–373 K, suggesting that adsorption of C_6H_6 is facile at low temperatures. Between 383 and 493 K, the MASI becomes predominantly CH_3OCH_3 , because C_6H_6 adsorption is less favorable at high temperatures. At temperatures above 473 K, $\text{CH}_3\text{-Z}$ species begin to appear on the surface (20–40%); however, the formation of $\text{CH}_3\text{-Z}$ is kinetically limited at low temperatures. Maximum rate analyses do not predict that $\text{CH}_3\text{-Z}$ species are the MASI between 353 and 493 K—only at temperatures above 503 K are $\text{CH}_3\text{-Z}$ species observed to cover the surface (Figure S13). This result agrees well with previous DFT studies in MFI that suggest that $\text{CH}_3\text{-Z}$ formation becomes more facile at high temperatures.³⁵

Previous experimental studies of $\text{C}_6\text{H}_6\text{-CH}_3\text{OCH}_3$ reactions used kinetic data, isotopic labeling studies, and postreaction titration studies to conclude that benzene methylates via the sequential pathway and that the arene alkylation step is rate determining on sites covered by $\text{CH}_3\text{-Z}$ species.²⁸ However, previous theoretical studies predict that concerted methylation is facile compared to the formation of $\text{CH}_3\text{-Z}$ species and that $\text{CH}_3\text{-Z}$ species are not a MASI at low temperatures.³⁵ Kinetic studies showed a linear dependence on benzene pressure (Figure 10), indicating that benzene adsorption occurs prior to

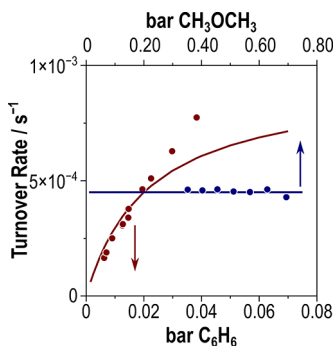
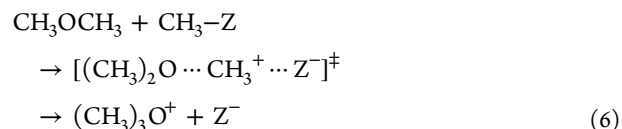


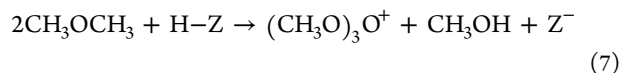
Figure 10. Comparison of DFT-obtained turnover rates with CH_3OCH_3 (solid) and experimentally obtained rates (circles) multiplied by a factor of 17 from ref 28. Data points are reported at 373 K, 0.02 bar C_6H_6 , 0.68 bar CH_3OCH_3 , and 0.1% aromatic conversion.

the rate-determining step, suggesting arene methylation is the rate-determining step.²⁸ However, we have shown that surface methylation also occurs after benzene adsorption as it is facilitated by coadsorbate interactions, which yields similar kinetic behavior (eqs S7 and S19). The zero-order dependence in CH_3OCH_3 pressure indicates that the MASI is derived from CH_3OCH_3 , such as $\text{CH}_3\text{OCH}_3^*$, $\text{CH}_3\text{-Z}$, or $\text{C}_6\text{H}_6\text{-CH}_3\text{OCH}_3^*$ (coadsorbed). Our DFT calculations, however, suggest that $\text{CH}_3\text{-Z}$ is never a MASI at these conditions, similar to previous theoretical work,³⁵ as it is quickly consumed by coadsorbed C_6H_6 and surface methylation never approaches equilibrium because of the low CH_3OH content (0.0002 bar). Isotopic studies demonstrate that when feeding d_0 and d_6

CH_3OCH_3 at benzene methylation conditions, there is 1:2:1 $d_0:d_3:d_6$, suggesting facile C–O bond cleavage, and our calculated barriers concur. However, the low CH_3OH content prevents scrambling via reversible surface methylation reactions and this scrambling is more likely explained by the formation and decomposition of trimethyloxonium species (TMO^+) through a sequential route:



or a concerted route



Both sequential and concerted trimethyloxonium formation occur with low barriers (124 and 60 kJ mol^{-1} for sequential and 80 kJ mol^{-1} for concerted TMO^+ formation). This indicates rapid exchange of CH_3 between CH_3OCH_3 and the zeolite surface, resulting in the observed $d_0:d_3:d_6$ ratios, as shown in Section S3. These TMO^+ species can also contribute to surface and ring methylation, further discussed in Section S3. Postreaction titration studies (H-SPP heated to 423 K to remove physisorbed species) with flowing H_2O form CH_3OH in a 1:1 ratio with Al content, indicating that the heated material was covered with CH_3OH^* or $\text{CH}_3\text{-Z}$, with the former being more likely.²⁸ The concentration of $\text{CH}_3\text{-Z}$, however, is very sensitive to the pressure of C_6H_6 , CH_3OH , and H_2O in the system. The heat treatment to remove physisorbed species could have created a surface covered in $\text{CH}_3\text{-Z}$; these purge treatments are typical of zeolite methylation protocols for this reason. Instead, our DFT calculations suggest that a mixture of $\text{CH}_3\text{OCH}_3^*$ and coadsorbed $\text{C}_6\text{H}_6\text{-CH}_3\text{OCH}_3^*$ dominates the surface at benzene methylation conditions; this is consistent with the observed zero-order pressure dependence in CH_3OCH_3 . However, this DFT analysis predicts sublinear kinetic behavior in C_6H_6 (rather than the linear behavior observed). This disagreement with experimental evidence is caused by the C_6H_6 binding free energy calculated here (-11 kJ mol^{-1}), which is approximately 4 kJ mol^{-1} more exothermic than that found from experiments.²⁸ Increasing the binding energy to -7 kJ mol^{-1} ad hoc results in a linear dependence on benzene pressure, consistent with measured kinetic data.²⁸ This thermodynamic correction does not cause $\text{CH}_3\text{-Z}$ to become a predicted MASI, however, because with these altered data $\text{CH}_3\text{OCH}_3^*$ are predicted as the lone MASI at benzene methylation conditions. This benzene-facilitated surface methylation pathway, which was not considered in previous theoretical³⁵ or experimental²⁸ studies, explains low $\text{CH}_3\text{-Z}$ coverages predicted by DFT and linear dependence on benzene pressure predicted by kinetic studies—thus bridging the gap between previous theoretical and experimental results.

3.3. Mechanisms of Toluene Methylation. Toluene methylation yields three unique products: *o*-, *m*-, and *p*-xylene. *p*-xylene has the highest industrial relevance as it is a precursor to terephthalic acid.⁶⁴ *m*-Xylene is typically thermodynamically favored;⁶⁵ however, zeolites, particularly H-ZSM-5, can shift this selectivity to favor *p*-xylene production through diffusive

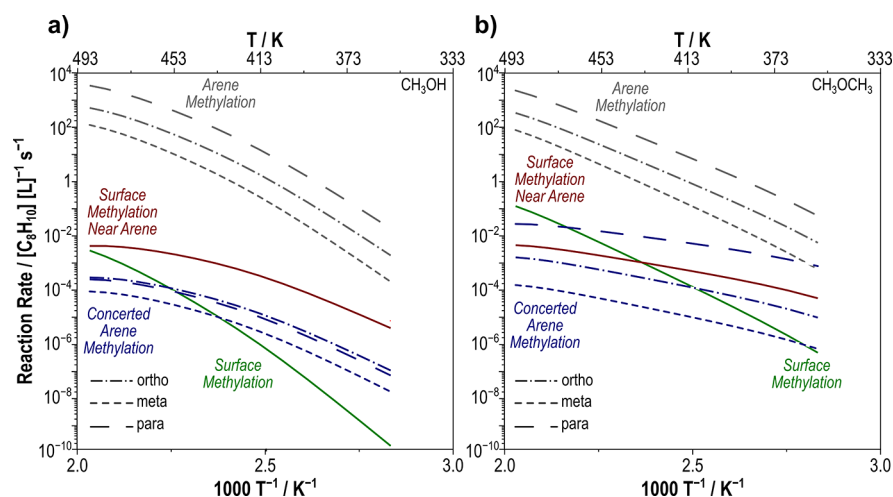


Figure 11. Maximum rates of sequential ring methylation (gray), surface methylation of O16 with benzene (red), surface methylation in an empty pore (green), and concerted methylation (blue) for *o*-, *m*-, and *p*-xylene formation with (a) CH₃OH and (b) CH₃OCH₃ at 0.03 bar C₇H₈, 0.68 bar CH₃OR, and 0.1% aromatic conversion, ranging from 353 to 493 K.

restrictions.^{66–69} Here, the mechanisms and rates of toluene methylation are analyzed using the previously discussed maximum rate analysis method to determine the intrinsic selectivities of the active site, uncorrupted by mass transport limitations (Figure 11). These insights can determine whether the observed preference for *p*-xylene is caused solely by mass transport limitations or if those limitations bolster a kinetically favored pathway.

Surface methylation in the presence of toluene demonstrates the same pore cooperativity as benzene (Section 3.2) to maximize noncovalent interactions and thus lower transition state barriers as compared to surface methylation in an empty pore. Surface methylation in the presence and absence of toluene occurs most favorably on O16. Toluene resides in the channel intersection and acts as a channel “cap” to maximize dispersive interactions (shown in Figure 12), and the surface methylation transition state resides in the straight channel to

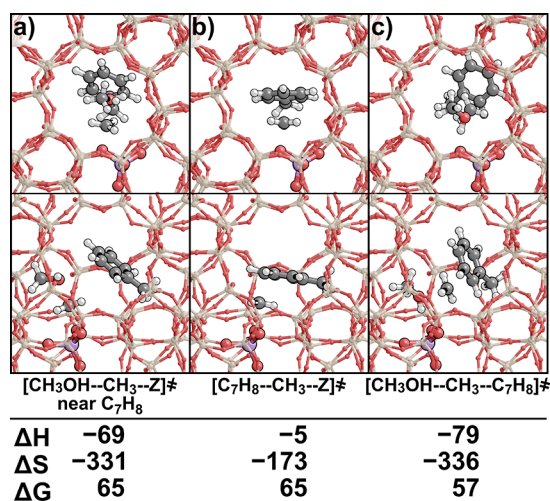


Figure 12. Lowest energy orientation for (a) surface methylation, (b) ring methylation (*para*-xylene formation shown), and (c) concerted methylation (*para*-xylene formation shown) with CH₃OCH₃ with views down the straight (top) and sinusoidal (bottom) channels. Enthalpy (kJ mol⁻¹), entropy (J K⁻¹ mol⁻¹), and free energy (kJ mol⁻¹) are reported at 403 K and relative to a proton on O14.

maximize favorable noncovalent interactions with the framework (such as H-bonding, cf., Figure 5). The presence of toluene lowers intrinsic barriers associated with CH₃OH surface methylation from 144 to 125 kJ mol⁻¹ (Figure 13); similarly, the barrier for methylation by CH₃OCH₃ decreases from 130 kJ mol⁻¹ to 115 kJ mol⁻¹ at 403 K and 1 bar of all species. At toluene methylation conditions (403 K, 0.03 bar C₇H₈, 0.68 bar CH₃OR, 0.1% aromatic conversion), surface methylation with spectating toluene occurs at a higher maximum rate than surface methylation in an empty pore. This suggests that CH₃-Z is primarily formed with spectating toluene at these conditions. However, at temperatures above 503 K for CH₃OH and 423 K for CH₃OCH₃, the rate of surface methylation in an empty pore occurs at a higher maximum rate than with spectating toluene. This likely occurs because strongly exothermic toluene adsorption (ΔH_{ads} of -94 kJ mol⁻¹) becomes balanced by entropic losses as the temperature increases. Surface methylation by CH₃OCH₃ occurs with rates only 1.5× faster than those with CH₃OH at 403 K, suggesting that CH₃OCH₃ and CH₃OH are equally capable of methylating the surface (Figure 11).

The rate of ring methylation via the sequential mechanism, like benzene methylation, occurs most favorably at O16 and has maximum rates >200× higher than those of surface methylation at toluene methylation conditions (Figure 11b), indicating that the rate of ring methylation is limited by the formation of surface methoxy species. Therefore, surface methylation with spectating toluene is the rate-determining step of the sequential mechanism with CH₃OH and CH₃OCH₃. Although ring methylation does not control the rate of sequential methylation, it does control the selectivity toward *o*-, *m*-, or *p*-xylene. Ring methylation selectivity favors *p*-xylene, then *o*-xylene, and finally *m*-xylene (Figure 11), suggesting that *p*-xylene is the kinetically preferred product of the sequential mechanism; this neglects additional effects of mass transport that would prevent egress of *o*- and *m*-xylene in practical studies. Such high *p*-xylene selectivity is not observed in experimental studies (573 K, 0.015 bar CH₃OH, 0.06 bar C₇H₈, and 4.3% C₇H₈ conversion) which have demonstrated that *p*-xylene formation is only slightly favored, with distributions of 35% *o*-, 28% *m*-, and 38% *p*-xylene.⁷⁰ At the same conditions, DFT results suggest the distribution is 13%

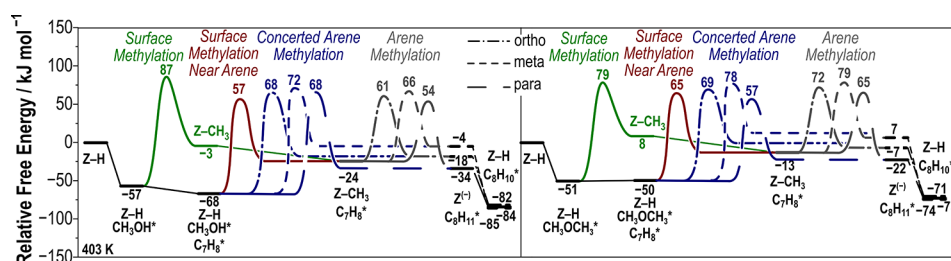


Figure 13. Reaction coordinate diagram of toluene methylation to form *o*-, *m*-, and *p*-xylene with CH_3OH (left) and CH_3OCH_3 (right) via the sequential (at O16) and concerted mechanisms. Free energy barriers are reported at 403 K, 1 bar.

o-, 4% *m*-, and 83% *p*-xylene; however, these distributions arise from arene methylation barriers that differ by only 12 kJ mol^{-1} (Figure 13), near the expected error in DFT calculations. Despite the uncertainties in these DFT-predicted selectivities, the trends suggested by DFT follow those found in experiment, where *p*-xylene is preferred over *o*-xylene and *m*-xylene. While DFT cannot accurately predict the selectivities of the products of these reactions, it can predict trends based on estimated free energy barriers and thus elucidate experimental results convoluted by mass transport limitations.

The concerted methylation of toluene has three possible transition states (forming each xylene) for each methylation agent, all of which H-bond with deprotonated O16 to stabilize the ROH leaving group. Here, intrinsic free energy barriers of concerted methylation can be directly compared to those of surface methylation with spectating toluene to determine the preferential toluene methylation route as both mechanisms demonstrate the same pressure dependencies. When CH_3OH serves as the methylation agent, surface methylation occurs with a lower barrier (125 kJ mol^{-1}) than concerted methylation to form *o*- (136 kJ mol^{-1}), *m*- (141 kJ mol^{-1}), and *p*-xylene (136 kJ mol^{-1}). The sequential mechanism occurs with barriers over 10 kJ mol^{-1} lower than those of the concerted mechanism when CH_3OH serves as the methylation agent, suggesting that sequential methylation is the predominant mechanism through which CH_3OH methylates toluene. When CH_3OCH_3 is the methylation agent, the barrier to methylate the surface (115 kJ mol^{-1}) is less than concerted barriers to form *o*- (119 kJ mol^{-1}) and *m*-xylene (128 kJ mol^{-1}) but higher than the concerted barrier to form *p*-xylene (107 kJ mol^{-1} , Figure 13). Therefore, when CH_3OCH_3 is the methylation agent, *p*-xylene is formed via the concerted mechanism preferentially over $\text{CH}_3\text{-Z}$ species and other xylene isomers. Barriers to form *p*-xylene are $7\text{--}21 \text{ kJ mol}^{-1}$ lower than those to form *o*- or *m*-xylene, indicating that the intrinsic selectivity favors the formation of *p*-xylene and its formation is likely further promoted by mass transport restrictions disfavoring the desorption of *o*- and *m*-xylene from the catalyst compared to the more-linear *para* isomer.

p-Xylene is the most favorable product to form for both CH_3OH and CH_3OCH_3 ; however, methylation to form *p*-xylene occurs through different mechanisms with CH_3OH (sequential methylation) and CH_3OCH_3 (concerted methylation), suggesting that the preferred methylation mechanism is dependent on both the position of methyl-addition and methylation agent. Neither CH_3OH nor CH_3OCH_3 has proven a noticeably superior methylating agent among all methylation locations examined thus far (benzene and toluene); DFT-predicted barriers for each species differ by $<20 \text{ kJ mol}^{-1}$ (Figure S14).

Similar to Section 3.2, surface MASI were calculated using a Langmuirian adsorption model with the same potential MASI, except with toluene instead of benzene (prediction of surface MASI are shown in Figure S15), and are demonstrated to be both temperature and methylation agent dependent. When CH_3OH is the methylation agent, $\text{C}_7\text{H}_8\text{-CH}_3\text{OH}^*$ is the MASI at temperatures below 413 K; however, as the temperature increases C_7H_8 adsorption becomes less favorable and the MASI becomes a mixture of $\text{C}_7\text{H}_8\text{-CH}_3\text{OH}^*$ and CH_3OH^* at temperatures above 413 K. As with benzene, entropic effects for larger arene species limit adsorption at higher temperatures, where high-entropy gas-phase species are favored. When CH_3OCH_3 is the methylation agent, $\text{CH}_3\text{OCH}_3^*$ is the MASI at all temperatures (353–493 K), because toluene does not adsorb as strongly next to CH_3OCH_3 ($\Delta G_{\text{ads}} = -50 \text{ kJ mol}^{-1}$) as it does near CH_3OH ($\Delta G_{\text{ads}} = -68 \text{ kJ mol}^{-1}$) (Figure 13).

The DFT results suggest that toluene methylation via CH_3OCH_3 likely occurs via a concerted mechanism with barriers $\sim 8 \text{ kJ mol}^{-1}$ lower than those of surface methylation. This value falls within the uncertainty of DFT, so it is difficult to determine which, if any, mechanism prevails at these conditions. Similar to benzene methylation, DFT-predictions can be used to provide insight and alternative explanations for previously published kinetic, surface titration, and isotopic switching results during CH_3OCH_3 and toluene coreaction conditions (403 K, 0.008–0.08 bar C_7H_8 , 0.68 bar CH_3OCH_3 , 0.1% conversion).²⁸ Experimental kinetic results predict no dependence on CH_3OCH_3 pressure and a linear dependence on toluene pressure, suggesting that the rate-determining step occurs after toluene adsorption, and thus the rate-determining step was toluene methylation. However, as we have shown with benzene and toluene methylation, surface methylation can occur in the presence of a spectating arene species, which explains the linear rate dependence on arene pressure. Furthermore, an abundance of $\text{CH}_3\text{OCH}_3^*$ on the surface explains a zero-order dependence on CH_3OCH_3 pressure. DFT results predict a linear dependence on toluene pressure and no dependence on CH_3OCH_3 pressure (Figure 14), confirming that this species is the MASI, consistent with these previous kinetic studies. Isotopic switching studies also demonstrated a 1:2:1 mixture of $d_0:d_3:d_6$ when d_0 and d_6 CH_3OCH_3 were cofed during toluene methylation.²⁸ Similar to benzene methylation, we suggest that this rapid exchange is likely to occur via trimethyloxonium species, not because surface methylation is a quasi-equilibrated step.

3.4. Mechanisms of Methylbenzene Methylation at Methanol-to-Hydrocarbon Conditions. Methanol-to-hydrocarbon (MTH) reactions typically occur at transient conditions because catalyst induction and deactivation

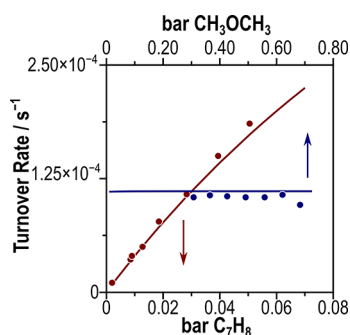


Figure 14. Comparison of DFT-obtained turnover rates with CH_3OCH_3 (solid) and experimentally obtained rates (circles) multiplied by a factor of 4 from ref 28. Data points are reported at 403 K, 0.03 bar C_7H_8 , 0.68 bar CH_3OCH_3 , and 0.1% aromatic conversion.

preclude steady state operation. Industrially, this is overcome by operating in fluidized bed reactors with low catalyst residence times. MTH occurs at higher temperatures (523–723 K) than arene methylation conditions (373–473 K, 0.1% conversion) and can form a range of substituted methylbenzene cocatalysts which produce light alkenes in the aromatic cycle.^{5,71,72} Here, we will analyze and interpret our arene methylation reactions at MTH conditions assuming 623 K, 0.04 bar C_xH_y , 0.08 bar CH_3OR , and 10% conversion, similar to previous studies of MTH.⁷¹

Surface methylation was the rate-determining step of the sequential mechanism at low-temperatures (373–473 K) and low conversions (<1%) and occurred near a spectating arene at benzene and toluene methylation conditions (373 and 403 K, respectively). However, this trend is not observed in the rates of surface methylation at higher temperatures and near larger arene species (C_{9+}). Surface methylation in an empty pore is the preferred mechanism for all species at MTH temperatures (near 623 K), because arenes are less likely to coadsorb at higher temperatures and larger arenes adsorb more weakly because of steric hindrance (Figure S16). Larger arenes, however, do not adsorb into zeolite voids during MTH; instead, they are formed within those intersections and their limited diffusivities render them effectively trapped as cocatalysts. As C_6 – C_{12} arenes will display a wide variety of diffusivities and adsorption energies, for the purposes of this section of the study, we consider all reactions taking place with or in the presence of a coadsorbed arene. For example, to methylate a C_{10} arene, we assume that CH_3OCH_3 must either react with the arene in a concerted manner or methylate the surface in its presence because the arene species cannot desorb.

The maximum rates of ring methylation are over 1000× greater than the maximum rates of surface methylation (near a coadsorbed arene) at MTH conditions for both CH_3OH and CH_3OCH_3 (Figure S17). Therefore, surface methylation is the rate-determining step for the sequential arene methylation pathway.

DFT-predicted rates of concerted methylation and sequential methylation pathways show no clear trends regarding the mechanism, and the favorability of mechanisms can switch based on the choice of methylation agent. For instance, when methylating 1,2,4-trimethylbenzene to 1,2,3,5-tetramethylbenzene with CH_3OH , the rate of concerted methylation is $\sim 100\times$ that of the sequential rate (correlating to a barrier difference of 18 kJ mol^{-1} , Figure S18); however, the same reaction with

CH_3OCH_3 occurs with sequential rates $\sim 70\times$ those of concerted methylation (corresponding to a barrier difference of 6 kJ mol^{-1} , Figure S18). Concerted methylation rates tend to be within 50× of each other for CH_3OH and CH_3OCH_3 (Figure S18), indicating that both species are viable methylating agents at MTH conditions. In general, the identity of the reactants dictates the preferred mechanism; for instance, all products of *o*-xylene methylation (Figure 1 shows the products) are formed via the concerted mechanism with CH_3OCH_3 at MTH conditions while all products of *m*-xylene are preferentially formed via the sequential mechanism at the same conditions; this trend of reactants preferring the same methylation mechanism holds true for all methylbenzene species investigated. Overall, it is difficult to use trends to predict the predominant mechanism and methylation agent of arene methylation. It is likely that both mechanisms contribute to the growth of aromatic species depending on the choice of methylation agent and number of spectating methyl-substituents.

The formation of higher methylbenzenes from benzene is of fundamental interest to determine active methylbenzene species during MTH reactions. Figure 15 shows the lowest

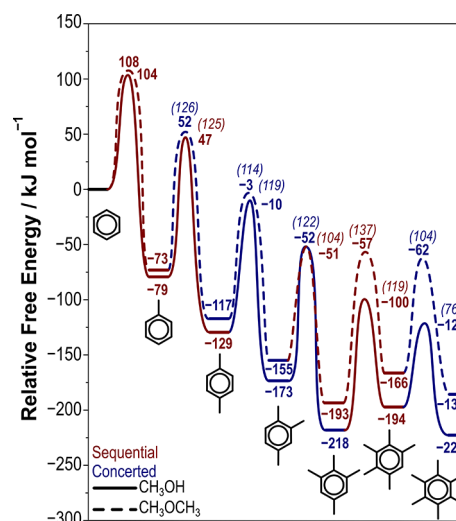


Figure 15. Reaction coordinate diagram of hexamethylbenzene formation via repeated benzene methylation with CH_3OH (solid lines) and CH_3OCH_3 (dashed lines). Overall barriers (relative to C_6H_6^*) are shown in bold, and intrinsic barriers are listed in italics and parentheses. Red lines indicate that the sequential mechanism is preferred, while blue lines indicate that the concerted mechanism is preferred. Barriers are reported at 623 K, 1 bar of all species.

methylation barriers and the most facile chemical pathways to reach hexamethylbenzene (structures shown in Section S6). The formation of hexamethylbenzene from benzene proceeds through *p*-xylene, 1,2,4-trimethylbenzene, and 1,2,3,5-tetramethylbenzene—all of which have been identified as possible intermediates of the aromatic cycle in MTH chemistry by previous DFT and kinetic studies.^{73–75} Figure 15 shows these pathways for methylation via CH_3OH and CH_3OCH_3 ; both species prefer to proceed through the same intermediates to form hexamethylbenzenes, though some methylations occur via different pathways (sequential or concerted). Intrinsic methylation barriers vary from 76–137 kJ mol^{-1} but show no systematic trends with the number of methyl-substituents on the ring; therefore, forming C_{10+} species is likely feasible during

MTH processes. This result contradicts previous theoretical studies which have predicted that methylation barriers decrease with additional methyl-substituents on the ring;³⁹ however, these studies were performed on zeolite cluster models and only investigated four ring interconversion pathways via the concerted mechanism—an insufficient analysis for these complicated pathways. The formation of higher methylbenzene species is thermodynamically favorable, with average reaction free energies of -34 kJ mol^{-1} . These reaction free energies increase with additional methyl substitution. For example, the formation of pentamethylbenzene from 1,2,3,5-tetramethylbenzene has a positive reaction free energy ($+24$ and $+27 \text{ kJ mol}^{-1}$ for CH_3OH and CH_3OCH_3 , respectively). This indicates that extensively substituted rings start to encounter steric hindrance within MFI intersections, consistent with their less favorable adsorption energies (Table S2). Despite this, methylation reactions are generally thermodynamically favorable and occur with barriers significantly lower than those reported for arene isomerization and alkene formation. During these methylation reactions, several competing factors affect the energies of guest species: electron withdrawing groups, steric hindrance, van der Waals interactions, and repulsive effects. The absence of a monotonic trend in methylation barriers suggests that none of these factors dominate in stabilizing or destabilizing methylation transition states; thus, interpolation of barriers in MFI yields inaccurate results because no dominant factor governs transition state energies during methylation reactions. Overall, the relatively low barriers of methylation indicate that arenes either escape zeolite domains as aromatic products of MTH or become extensively substituted as C_{10} – C_{12} species that are trapped within MFI intersections. These highly substituted arenes serve as cocatalysts in the aromatic cycle and produce light alkenes.^{18,20,71,72,76–79} The formation of geminal methylated aromatic species is shown to be an important step in the aromatics-cycle of MTO. Previous reports comparing methylation and geminal methylation in H-ZSM-12 and H-ZSM-22 suggest that geminal methylation barriers are only competitive with methylation barriers for C_{10+} species;³⁸ similar results have been demonstrated in CHA, BEA, and H-ZSM-5.^{19,80,81} Here, we find that barriers of geminal methylation via the sequential mechanism are 50 – 90 kJ mol^{-1} higher those of monomethylation (Figure S19). These results further support that large aromatic rings are cocatalyzing the formation of alkenes via the aromatic cycle. These large aromatic rings will ultimately grow to polyaromatic species^{82–84} via deactivation mechanisms when trapped in zeolite pores.

4. CONCLUSIONS

Reactant, product, and transition state species involved in arene methylation reactions were systematically reoriented to probe the potential energy surface in an attempt to identify their respective global minima. These reorientations demonstrate that a single optimization of a user-generated structure is insufficient to obtain reliable ground state energies. Reorientations reduced energies by up to 45 kJ mol^{-1} for states tested here. Furthermore, these systematic reorientations provide valuable insight regarding the void and coadsorbate cooperativity, which are not immediately apparent. Through systematic reorientations of surface methylation transition states with coadsorbed arenes, we have demonstrated that MFI offers a unique environment for catalysis because small transition states (e.g., surface methylation) can reside in the

straight channel to maximize dispersive interactions while larger arenes (e.g., benzene) can reside in the channel intersection to minimize repulsive interactions with the zeolite framework. The proximity and locations of these species creates a “capped” channel which resembles a side-pocket in which surface methylation is accelerated by noncovalent interactions among coadsorbates and by solvation by the zeolite framework. This cooperativity of pores makes MFI an ideal catalyst for housing transition states of different sizes, such as those in BTX methylation and MTH reactions.

Concerted and sequential arene methylations were studied with CH_3OH and CH_3OCH_3 for all methylbenzene interconversion pathways from benzene to hexamethylbenzene. Maximum rate analyses were used to determine the rate-determining steps of the sequential mechanism, compare the sequential and concerted mechanism, and compare DFT-predicted rates to previous kinetic studies. Benzene methylation is predicted to occur via sequential methylation at reasonable temperatures (353 – 623 K) and pressures (0.02 – 1 bar). Surface methylation facilitated by coadsorbed benzene is rate-determining at these conditions with low benzene conversion (0.1%). However, at higher ROH pressures (caused by higher conversions, above 20%), the rate of surface methylation approaches equilibrium, thus limiting the rate of the subsequent arene methylation reaction and causing it to become rate-determining. DFT data demonstrate that coadsorbed benzene facilitates surface methylation by CH_3OH and CH_3OCH_3 , resulting in rates that yield pressure dependencies identical to those observed experimentally. Additionally, isotopically labeled methyl groups in CH_3OCH_3 can be scrambled through trimethyloxonium cations, and surface methoxy species are only MASI in the absence of CH_3OH , H_2O , and C_6H_6 (i.e., can only be formed at high coverages by heating or flowing in an inert gas). These calculations shed new light on prior experimental studies leading to a more thorough understanding of BTX methylation reactions.

Concerted and sequential barriers tend to be within 20 kJ mol^{-1} of each other for the complete set of arene methylation reactions (from benzene to hexamethylbenzene), indicating that both mechanisms likely occur. Similarly, barriers for methylation by CH_3OH and CH_3OCH_3 are nearly identical, suggesting that either species can methylate arenes and that CH_3OH formed by CH_3OCH_3 reactions may itself react to form H_2O . Intrinsic methylation free energy barriers remain between 76 and 137 kJ mol^{-1} during repeated methylation of benzene to hexamethylbenzene, suggesting that the number of methyl-substituents on the ring has no consistent trend with regard to raising or lowering activation barriers of methylation. Additionally, reaction free energies become less negative but generally remain low, suggesting that the formation of C_{10} – C_{12} species is unlikely kinetically limited during MTH reactions. This suggests that an aromatic compound, once formed during MTH, likely either desorbs from the zeolite as a light aromatic product (C_6 – C_8) or forms an extensively methylated species, such as tetra-, penta-, or hexamethylbenzene. This extensively methylated arene will serve as a cocatalyst for olefin production and eventually lead to catalyst deactivation via the formation of polyaromatic species. Overall, this study provides mechanistic understanding of low-temperature BTX alkylations and gives insight into the dominant aromatic species present during MTH reactions while employing a novel method of identifying global minima and stable transition state structures within

zeolite frameworks and revealing previously undescribed cooperativity between zeolite voids that enable the versatile chemistry of the MFI framework.

■ ASSOCIATED CONTENT

Supporting Information

The Supporting Information is available free of charge on the ACS Publications website at DOI: [10.1021/acscatal.9b00650](https://doi.org/10.1021/acscatal.9b00650).

Formulas and details of frequency calculations for enthalpy and free energy approximations, detailed images showing structures and reorientation schemes, derivations for arene methylation rate equations, and all activation and reaction enthalpies and entropies (PDF)

■ AUTHOR INFORMATION

Corresponding Author

*E-mail: hibbitts@che.ufl.edu.

ORCID

Alexander Hoffman: [0000-0002-1337-9297](https://orcid.org/0000-0002-1337-9297)

David Hibbitts: [0000-0001-8606-7000](https://orcid.org/0000-0001-8606-7000)

Notes

The authors declare no competing financial interest.

■ ACKNOWLEDGMENTS

This work was funded by an ACS Petroleum Research Fund New Doctoral Investigation Award (57079-DN15). Computational resources were provided by the Extreme Science and Engineering Discovery Environment (XSEDE),⁸⁵ which is supported by National Science Foundation grant number ACI-1548562 through allocation CTS160041. Additional computational resources were provided by University of Florida Research Computing.

■ REFERENCES

- (1) Jones, A. J.; Iglesia, E. Kinetic, Spectroscopic, and Theoretical Assessment of Associative and Dissociative Methanol Dehydration Routes in Zeolites. *Angew. Chem., Int. Ed.* **2014**, *53*, 12177–12181.
- (2) Ghorbanpour, A.; Rimer, J. D.; Grabow, L. C. Computational Assessment of the Dominant Factors Governing the Mechanism of Methanol Dehydration over H-ZSM-5 with Heterogeneous Aluminum Distribution. *ACS Catal.* **2016**, *6*, 2287–2298.
- (3) Sarazen, M. L.; Doslak, E.; Iglesia, E. Effects of Void Environment and Acid Strength on Alkene Oligomerization Selectivity. *ACS Catal.* **2016**, *6*, 7059–7070.
- (4) Wang, S.; Agirrezabal-Telleria, I.; Bhan, A.; Simonetti, D.; Takanabe, K.; Iglesia, E. Catalytic Routes to Fuels from C1 and Oxygenate Molecules. *Faraday Discuss.* **2017**, *197*, 9–39.
- (5) Ilias, S.; Bhan, A. Mechanism of the Catalytic Conversion of Methanol to Hydrocarbons. *ACS Catal.* **2013**, *3*, 18–31.
- (6) Van Speybroeck, V.; Van der Mynsbrugge, J.; Vandichel, M.; Hemelsoet, K.; Lesthaeghe, D.; Ghysels, A.; Marin, G. B.; Waroquier, M. First Principle Kinetic Studies of Zeolite-catalyzed Methylation Reactions. *J. Am. Chem. Soc.* **2011**, *133*, 888–899.
- (7) Qi, L.; Wei, Y.; Xu, L.; Liu, Z. Reaction Behaviors and Kinetics During Induction Period of Methanol Conversion on HZSM-5 Zeolite. *ACS Catal.* **2015**, *5*, 3973–3982.
- (8) Blaszkowski, S. R.; van Santen, R. A. Theoretical Study of C–C Bond Formation in the Methanol-to-Gasoline Process. *J. Am. Chem. Soc.* **1997**, *119*, 5020–5027.
- (9) Wei, Z.; Chen, Y.-Y.; Li, J.; Guo, W.; Wang, S.; Dong, M.; Qin, Z.; Wang, J.; Jiao, H.; Fan, W. Stability and Reactivity of Intermediates of Methanol Related Reactions and C–C Bond Formation over H-ZSM-5 Acidic Catalyst: A Computational Analysis. *J. Phys. Chem. C* **2016**, *120*, 6075–6087.
- (10) Brogaard, R. Y.; Henry, R.; Schuurman, Y.; Medford, A. J.; Moses, P. G.; Beato, P.; Svelle, S.; Nørskov, J. K.; Olsbye, U. Methanol-to-hydrocarbons Conversion: The Alkene Methylation Pathway. *J. Catal.* **2014**, *314*, 159–169.
- (11) Svelle, S.; Kolboe, S.; Swang, O.; Olsbye, U. Methylation of Alkenes and Methylbenzenes by Dimethyl Ether or Methanol on Acidic Zeolites. *J. Phys. Chem. B* **2005**, *109*, 12874–12878.
- (12) Svelle, S.; Visur, M.; Olsbye, U.; Saepurahman; Bjørgen, M. Mechanistic Aspects of the Zeolite Catalyzed Methylation of Alkenes and Aromatics with Methanol: A Review. *Top. Catal.* **2011**, *54*, 897–906.
- (13) Svelle, S.; Arstad, B.; Kolboe, S.; Swang, O. A Theoretical Investigation of the Methylation of Alkenes with Methanol over Acidic Zeolites. *J. Phys. Chem. B* **2003**, *107*, 9281–9289.
- (14) Hwang, A.; Prieto-Centurion, D.; Bhan, A. Isotopic Tracer Studies of Methanol-to-olefins Conversion over HSAPO-34: The Role of the Olefins-based Catalytic Cycle. *J. Catal.* **2016**, *337*, 52–56.
- (15) Lesthaeghe, D.; Van der Mynsbrugge, J.; Vandichel, M.; Waroquier, M.; Van Speybroeck, V. Full Theoretical Cycle for Both Ethene and Propene Formation During Methanol-to-Olefin Conversion in H-ZSM-5. *ChemCatChem* **2011**, *3*, 208–212.
- (16) Joshi, Y. V.; Bhan, A.; Thomson, K. T. DFT-Based Reaction Pathway Analysis of Hexadiene Cyclization via Carbenium Ion Intermediates: Mechanistic Study of Light Alkane Aromatization Catalysis. *J. Phys. Chem. B* **2004**, *108*, 971–980.
- (17) Mullen, G. M.; Janik, M. J. Density Functional Theory Study of Alkane-Alkoxide Hydride Transfer in Zeolites. *ACS Catal.* **2011**, *1*, 105–115.
- (18) Ilias, S.; Khare, R.; Malek, A.; Bhan, A. A Descriptor for the Relative Propagation of the Aromatic- and Olefin-based Cycles in Methanol-to-hydrocarbons Conversion on H-ZSM-5. *J. Catal.* **2013**, *303*, 135–140.
- (19) Lesthaeghe, D.; Horré, A.; Waroquier, M.; Marin, G. B.; Van Speybroeck, V. Theoretical Insights on Methylbenzene Side-chain Growth in ZSM-5 Zeolites for Methanol-to-olefin Conversion. *Chem. - Eur. J.* **2009**, *15*, 10803–10808.
- (20) Arstad, B.; Nicholas, J. B.; Haw, J. F. Theoretical Study of the Methylbenzene Side-chain Hydrocarbon Pool Mechanism in Methanol to Olefin Catalysis. *J. Am. Chem. Soc.* **2004**, *126*, 2991–3001.
- (21) Wang, C.; Xu, J.; Qi, G.; Gong, Y.; Wang, W.; Gao, P.; Wang, Q.; Feng, N.; Liu, X.; Deng, F. Methylbenzene Hydrocarbon Pool in Methanol-to-olefins Conversion over Zeolite H-ZSM-5. *J. Catal.* **2015**, *332*, 127–137.
- (22) Odedairo, T.; Balasamy, R. J.; Al-Khattaf, S. Toluene Disproportionation and Methylation over Zeolites TNU-9, SSZ-33, ZSM-5, and Mordenite Using Different Reactor Systems. *Ind. Eng. Chem. Res.* **2011**, *50*, 3169–3183.
- (23) Beschmann, K.; Riekert, L. Isomerization of Xylene and Methylation of Toluene on Zeolite H-ZSM-5. Compound Kinetics and Selectivity. *J. Catal.* **1993**, *141*, 548–565.
- (24) Cha, S. H.; Hong, S. B. Reaction Intermediates and Mechanism of the Zeolite-catalyzed Transalkylation of 1,2,4-trimethylbenzene with Toluene. *J. Catal.* **2018**, *357*, 1–11.
- (25) Vos, A. M.; Rozanska, X.; Schoonheydt, R. A.; van Santen, R. A.; Hutschka, F.; Hafner, J. A Theoretical Study of the Alkylation Reaction of Toluene with Methanol Catalyzed by Acidic Mordenite. *J. Am. Chem. Soc.* **2001**, *123*, 2799–2809.
- (26) Wen, Z.; Yang, D.; He, X.; Li, Y.; Zhu, X. Methylation of Benzene with Methanol over HZSM-11 and HZSM-5: A Density Functional Theory Study. *J. Mol. Catal. A: Chem.* **2016**, *424*, 351–357.
- (27) Saepurahman; Visur, M.; Olsbye, U.; Bjørgen, M.; Svelle, S. In Situ FT-IR Mechanistic Investigations of the Zeolite Catalyzed Methylation of Benzene with Methanol: H-ZSM-5 Versus H-beta. *Top. Catal.* **2011**, *54*, 1293–1301.
- (28) Hill, I.; Malek, A.; Bhan, A. Kinetics and Mechanism of Benzene, Toluene, and Xylene Methylation over H-MFI. *ACS Catal.* **2013**, *3*, 1992–2001.

- (29) Hill, I. M.; Hashimi, S. A.; Bhan, A. Kinetics and Mechanism of Olefin Methylation Reactions on Zeolites. *J. Catal.* **2012**, *285*, 115–123.
- (30) Svelle, S.; Ronning, P.; Olsbye, U.; Kolboe, S. Kinetic Studies of Zeolite-catalyzed Methylation Reactions. Part 2. Co-reaction of [12C]propene or [12C]n-butene and [13C]methanol. *J. Catal.* **2005**, *234*, 385–400.
- (31) Svelle, S.; Rønning, P. O.; Kolboe, S. Kinetic Studies of Zeolite-catalyzed Methylation Reactions I. Coreaction of [12C]ethene and [13C]methanol. *J. Catal.* **2004**, *224*, 115–123.
- (32) Vos, A. M.; Nulens, K. H. L.; De Proft, F.; Schoonheydt, R. A.; Geerlings, P. Reactivity Descriptors and Rate Constants for Electrophilic Aromatic Substitution: Acid Zeolite Catalyzed Methylation of Benzene and Toluene. *J. Phys. Chem. B* **2002**, *106*, 2026–2034.
- (33) Moors, S. L. C.; De Wispelaere, K.; Van der Mynsbrugge, J.; Waroquier, M.; Van Speybroeck, V. Molecular Dynamics Kinetic Study on the Zeolite-Catalyzed Benzene Methylation in ZSM-5. *ACS Catal.* **2013**, *3*, 2556–2567.
- (34) Gomes, J.; Zimmerman, P. M.; Head-Gordon, M.; Bell, A. T. Accurate Prediction of Hydrocarbon Interactions with Zeolites Utilizing Improved Exchange-Correlation Functionals and QM/MM Methods: Benchmark Calculations of Adsorption Enthalpies and Application to Ethene Methylation by Methanol. *J. Phys. Chem. C* **2012**, *116*, 15406–15414.
- (35) De Wispelaere, K.; Martínez-Espín, J. S.; Hoffmann, M. J.; Svelle, S.; Olsbye, U.; Bligaard, T. Understanding Zeolite-catalyzed Benzene Methylation Reactions by Methanol and Dimethyl Ether at Operating Conditions from First Principle Microkinetic Modeling and Experiments. *Catal. Today* **2018**, *312*, 35–43.
- (36) Martínez-Espín, J. S.; Mortén, M.; Janssens, T. V. W.; Svelle, S.; Beato, P.; Olsbye, U. New Insights into Catalyst Deactivation and Product Distribution of Zeolites in the Methanol-to-hydrocarbons (MTH) Reaction with Methanol and Dimethyl Ether Feeds. *Catal. Sci. Technol.* **2017**, *7*, 2700–2716.
- (37) Martínez-Espín, J. S.; De Wispelaere, K.; Westgård Erichsen, M.; Svelle, S.; Janssens, T. V. W.; Van Speybroeck, V.; Beato, P.; Olsbye, U. Benzene Co-reaction with Methanol and Dimethyl Ether over Zeolite and Zeotype Catalysts: Evidence of Parallel Reaction Paths to Toluene and Diphenylmethane. *J. Catal.* **2017**, *349*, 136–148.
- (38) Chu, Y.; Sun, X.; Yi, X.; Ding, L.; Zheng, A.; Deng, F. Slight Channel Difference Influences the Reaction Pathway of Methanol-to-olefins Conversion over Acidic H-ZSM-22 and H-ZSM-12 Zeolites. *Catal. Sci. Technol.* **2015**, *5*, 3507–3517.
- (39) Arstad, B.; Kolboe, S.; Swang, O. A Theoretical Investigation on the Methylation of Methylbenzenes on Zeolites. *J. Phys. Chem. B* **2002**, *106*, 12722–12726.
- (40) Kresse, G.; Hafner, J. *Ab Initio* Molecular Dynamics for Liquid Metals. *Phys. Rev. B: Condens. Matter Mater. Phys.* **1993**, *47*, 558–561.
- (41) Kresse, G.; Hafner, J. *Ab Initio* Molecular-dynamics Simulation of the Liquid-metal-amorphous-semiconductor Transition in Germanium. *Phys. Rev. B: Condens. Matter Mater. Phys.* **1994**, *49*, 14251–14269.
- (42) Kresse, G.; Furthmüller, J. Efficient Iterative Schemes for *Ab Initio* Total-energy Calculations Using a Plane-wave Basis Set. *Phys. Rev. B: Condens. Matter Mater. Phys.* **1996**, *54*, 11169–11186.
- (43) Kresse, G.; Furthmüller, J. Efficiency of *Ab-initio* Total Energy Calculations for Metals and Semiconductors Using a Plane-wave Basis Set. *Comput. Mater. Sci.* **1996**, *6*, 15–50.
- (44) Blöchl, P. E. Projector Augmented-wave Method. *Phys. Rev. B: Condens. Matter Mater. Phys.* **1994**, *50*, 17953–17979.
- (45) Kresse, G.; Joubert, D. From Ultrasoft Pseudopotentials to the Projector Augmented-wave Method. *Phys. Rev. B: Condens. Matter Mater. Phys.* **1999**, *59*, 1758–1775.
- (46) Perdew, J. P.; Burke, K.; Ernzerhof, M. Generalized Gradient Approximation Made Simple. *Phys. Rev. Lett.* **1996**, *77*, 3865–3868.
- (47) Zhang, Y.; Yang, W. Comment on “Generalized Gradient Approximation Made Simple. *Phys. Rev. Lett.* **1998**, *80*, 890–890.
- (48) Hammer, B.; Hansen, L. B.; Nørskov, J. K. Improved Adsorption Energetics Within Density-functional Theory Using Revised Perdew-Burke-Ernzerhof Functionals. *Phys. Rev. B: Condens. Matter Mater. Phys.* **1999**, *59*, 7413–7421.
- (49) Grimme, S.; Ehrlich, S.; Goerigk, L. Effect of the Damping Function in Dispersion Corrected Density Functional Theory. *J. Comput. Chem.* **2011**, *32*, 1456–1465.
- (50) Schröder, H.; Creon, A.; Schwabe, T. Reformulation of the D3(Becke-Johnson) Dispersion Correction Without Resorting to Higher Than C₆ Dispersion Coefficients. *J. Chem. Theory Comput.* **2015**, *11*, 3163–3170.
- (51) Grimme, S.; Antony, J.; Ehrlich, S.; Krieg, H. A Consistent and Accurate *Ab Initio* Parametrization of Density Functional Dispersion Correction (DFT-D) for the 94 Elements H-Pu. *J. Chem. Phys.* **2010**, *132*, 154104.
- (52) Monkhorst, H. J.; Pack, J. D. Special Points for Brillouin-zone Integrations. *Phys. Rev. B* **1976**, *13*, 5188–5192.
- (53) Baerlocher, C.; McCusker, L. B. Database of Zeolite Structures: <http://www.iza-structure.org/databases>. 2013.
- (54) Hoffman, A.; DeLuca, M.; Hibbitts, D. Restructuring of MFI Framework Zeolite Models and Their Associated Artifacts in DFT Calculations. *J. Phys. Chem. C* **2019**, *123*, 6572.
- (55) Jónsson, H.; Mills, G.; Jacobsen, K. W. Nudged Elastic Band Method for Finding Minimum Energy Paths of Transitions. In *Classical and Quantum Dynamics in Condensed Phase Simulations*; Berne, B. J., Ciccotti, G., Coker, D. F., Eds.; World Scientific: 1998; pp 385–404.
- (56) Henkelman, G.; Jónsson, H. Improved Tangent Estimate in the Nudged Elastic Band Method for Finding Minimum Energy Paths and Saddle Points. *J. Chem. Phys.* **2000**, *113*, 9978–9985.
- (57) Henkelman, G.; Jónsson, H. A Dimer Method for Finding Saddle Points on High Dimensional Potential Surfaces Using Only First Derivatives. *J. Chem. Phys.* **1999**, *111*, 7010–7022.
- (58) Herrmann, S.; Iglesia, E. Elementary Steps in Acetone Condensation Reactions Catalyzed by Aluminosilicates with Diverse Void Structures. *J. Catal.* **2017**, *346*, 134–153.
- (59) Zhi, Y.; Shi, H.; Mu, L.; Liu, Y.; Mei, D.; Camaioni, D. M.; Lercher, J. A. Dehydration Pathways of 1-Propanol on HZSM-5 in the Presence and Absence of Water. *J. Am. Chem. Soc.* **2015**, *137*, 15781–15794.
- (60) Nystrom, S.; Hoffman, A.; Hibbitts, D. Tuning Brønsted Acid Strength by Altering Site Proximity in CHA Framework Zeolites. *ACS Catal.* **2018**, *8*, 7842–7860.
- (61) Flaherty, D. W.; Iglesia, E. Transition-state Enthalpy and Entropy Effects on Reactivity and Selectivity in Hydrogenolysis of N-alkanes. *J. Am. Chem. Soc.* **2013**, *135*, 18586–18599.
- (62) Flaherty, D. W.; Hibbitts, D. D.; Gürbüz, E. I.; Iglesia, E. Theoretical and Kinetic Assessment of the Mechanism of Ethane Hydrogenolysis on Metal Surfaces Saturated with Chemisorbed Hydrogen. *J. Catal.* **2014**, *311*, 350–356.
- (63) Flaherty, D. W.; Hibbitts, D. D.; Iglesia, E. Metal-catalyzed C-C Bond Cleavage in Alkanes: Effects of Methyl Substitution on Transition-state Structures and Stability. *J. Am. Chem. Soc.* **2014**, *136*, 9664–9676.
- (64) Vinek, H.; Lercher, J. A. Production and Reactions of Xylenes over H-ZSM5. *J. Mol. Catal.* **1991**, *64*, 23–39.
- (65) Chirico, R. D.; Steele, W. V. Thermodynamic Equilibria in Xylene Isomerization. 5. Xylene Isomerization Equilibria from Thermodynamic Studies and Reconciliation of Calculated and Experimental Product Distributions[†]. *J. Chem. Eng. Data* **1997**, *42*, 784–790.
- (66) Gobin, O. C.; Reitmeier, S. J.; Jentys, A.; Lercher, J. A. Diffusion Pathways of Benzene, Toluene and p-xylene in MFI. *Microporous Mesoporous Mater.* **2009**, *125*, 3–10.
- (67) Pope, C. G. Sorption of Benzene, Toluene and p-xylene on ZSM-5. *J. Phys. Chem.* **1984**, *88*, 6312–6313.
- (68) Kaeding, W. Selective Alkylation of Toluene with Methanol to Produce para-Xylene. *J. Catal.* **1981**, *67*, 159–174.

(69) Kaeding, W. Shape-selective Reactions with Zeolite Catalysts II. Selective Disproportionation of Toluene to Produce Benzene and p-Xylene. *J. Catal.* **1981**, *69*, 392–398.

(70) Ahn, J. H.; Kolvenbach, R.; Gutiérrez, O. Y.; Al-Khattaf, S. S.; Jentys, A.; Lercher, J. A. Tailoring P-xylene Selectivity in Toluene Methylation on Medium Pore-size Zeolites. *Microporous Mesoporous Mater.* **2015**, *210*, 52–59.

(71) Ilias, S.; Bhan, A. The Mechanism of Aromatic Dealkylation in Methanol-to-hydrocarbons Conversion on H-ZSM-5: What Are the Aromatic Precursors to Light Olefins? *J. Catal.* **2014**, *311*, 6–16.

(72) Wang, C.-M.; Wang, Y.-D.; Liu, H.-X.; Yang, G.; Du, Y.-J.; Xie, Z.-K. Aromatic-based Hydrocarbon Pool Mechanism for Methanol-to-olefins Conversion in H-SAPO-18: A Van Der Waals Density Functional Study. *Chinese Journal of Catalysis* **2015**, *36*, 1573–1579.

(73) Dessau, R. On the Mechanism of Methanol Conversion to Hydrocarbons over HZSM-5. *J. Catal.* **1982**, *78*, 136–141.

(74) Ilias, S.; Bhan, A. Tuning the Selectivity of Methanol-to-hydrocarbons Conversion on H-ZSM-5 by Co-processing Olefin or Aromatic Compounds. *J. Catal.* **2012**, *290*, 186–192.

(75) Wang, C.-M.; Wang, Y.-D.; Xie, Z.-K. Verification of the Dual Cycle Mechanism for Methanol-to-olefin Conversion in HSAPO-34: a Methylbenzene-based Cycle from DFT Calculations. *Catal. Sci. Technol.* **2014**, *4*, 2631–2638.

(76) Ma, H.; Chen, Y.; Wang, S.; Wei, Z.; Qin, Z.; Dong, M.; Li, J.; Fan, W.; Wang, J. Reaction Mechanism for the Conversion of Methanol to Olefins over H-ITQ-13 Zeolite: a Density Functional Theory Study. *Catal. Sci. Technol.* **2018**, *8*, 521–533.

(77) Wang, S.; Chen, Y.-Y.; Wei, Z.; Qin, Z.; Ma, H.; Dong, M.; Li, J.; Fan, W.; Wang, J. Polymethylbenzene or Alkene Cycle? Theoretical Study on Their Contribution to the Process of Methanol to Olefins over H-ZSM-5 Zeolite. *J. Phys. Chem. C* **2015**, *119*, 28482–28498.

(78) Wang, S.; Chen, Y.; Wei, Z.; Qin, Z.; Liang, T.; Dong, M.; Li, J.; Fan, W.; Wang, J. Evolution of Aromatic Species in Supercages and Its Effect on the Conversion of Methanol to Olefins over H-MCM-22 Zeolite: A Density Functional Theory Study. *J. Phys. Chem. C* **2016**, *120*, 27964–27979.

(79) Wang, S.; Chen, Y.; Qin, Z.; Zhao, T.-S.; Fan, S.; Dong, M.; Li, J.; Fan, W.; Wang, J. Origin and Evolution of the Initial Hydrocarbon Pool Intermediates in the Transition Period for the Conversion of Methanol to Olefins over H-ZSM-5 Zeolite. *J. Catal.* **2019**, *369*, 382–395.

(80) Lesthaeghe, D.; De Sterck, B.; Van Speybroeck, V.; Marin, G. B.; Waroquier, M. Zeolite Shape-selectivity in the Gem-methylation of Aromatic Hydrocarbons. *Angew. Chem., Int. Ed.* **2007**, *46*, 1311–1314.

(81) McCann, D. M.; Lesthaeghe, D.; Kletnieks, P. W.; Guenther, D. R.; Hayman, M. J.; Van Speybroeck, V.; Waroquier, M.; Haw, J. F. A Complete Catalytic Cycle for Supramolecular Methanol-to-olefins Conversion by Linking Theory with Experiment. *Angew. Chem., Int. Ed.* **2008**, *47*, 5179–5182.

(82) Mores, D.; Kornatowski, J.; Olsbye, U.; Weckhuysen, B. M. Coke Formation During the Methanol-to-olefin Conversion: In Situ Microspectroscopy on Individual H-ZSM-5 Crystals with Different Brønsted Acidity. *Chem. - Eur. J.* **2011**, *17*, 2874–2884.

(83) Rojo-Gama, D.; Signorile, M.; Bonino, F.; Bordiga, S.; Olsbye, U.; Lillerud, K. P.; Beato, P.; Svelle, S. Structure–deactivation Relationships in Zeolites During the Methanol-to-hydrocarbons Reaction: Complementary Assessments of the Coke Content. *J. Catal.* **2017**, *351*, 33–48.

(84) Bjørgen, M.; Olsbye, U.; Kolboe, S. Coke Precursor Formation and Zeolite Deactivation: Mechanistic Insights from Hexamethylbenzene Conversion. *J. Catal.* **2003**, *215*, 30–44.

(85) Towns, J.; Cockerill, T.; Dahan, M.; Foster, I.; Gaither, K.; Grimshaw, A.; Hazlewood, V.; Lathrop, S.; Lifka, D.; Peterson, G. D.; Roskies, R.; Scott, J. R.; Wilkens-Diehr, N. XSEDE: Accelerating Scientific Discovery. *Comput. Sci. Eng.* **2014**, *16*, 62–74.